at instant (1) is in upward motion, whereas at instant (2) it is in downward motion. As can be seen, the flow features at these times are quite different from each other. The surface pressure at instant (1) is much higher than that at instant (2) owing to the upward ramp motion (compressive stroke) though the shock wave is in formation stage. On the contrary, the shock wave at instant (2) is sharp. However, the surface pressure is much lower since the ramp moves downard (expansion stroke). When the ramp moved further downward so that the wedge angle became negative, an expansion fan was observed. When the ramp moved upward from −20 deg, we observed compression waves emanating from the surface and an expansion fan centered about the corner of the wedge.

Summary

Through numerical study using a moving grid system, inviscid supersonic flow past a moving compression ramp was investigated. The study revealed that the unsteady flow of the moving ramp could be considered steady or quasi-steady when $\bar{\Omega}$ was of order 0.01 or smaller. When $\bar{\Omega}$ was 0.1, the flow exhibited distinct unsteady behavior. The shock wave formed during the ramp motion was curved rather than straight. The surface pressure during the ramp motion was higher than the steady state value of the corresponding steady ramp. After the ramp motion ceased, it took a considerable time for the pressure to relax to the steady state value. When $\bar{\Omega} = 1.0$, the shock wave development was confined in the narrow region close to the moving surface. This shock wave then gradually moved away from the wall after the ramp stop and was finally developed to that of the steady state. When the ramp moved cyclically from −20 to 20 deg, hysteretic behavior of the flow was noticed.

References

[1]Degani, D., and Steger, J. L., "Comparison Between Navier-Stokes and Thin-Layer Computations for Separated Supersonic Flow," *AIAA Journal*, Vol. 21, No. 11, 1983, pp. 1604–1606.

[2]Hoffmann, K. A., *Computational Fluid Dynamics for Engineers, Engineering Education System*, Austin, TX, 1989, pp.402–403

[3]Kang, I. M. and Chang, K. S., "Euler Analysis of Transonic Stator-Rotor Interaction using a Finite Volume Method," *International Journal of Numerical Methods in Fluids*, Vol. 12, No. 7, 1991, pp. 625–636.

[4]Jameson, A., Schmidt, W., and Turkel, E., "Numerical Solutions of the Euler Equations by Finite Volume Methods using Runge-Kutta Time Stepping Schemes," AIAA Paper 81-1259, June 1981.

[5]Pulliam, T. H., "Artificial Dissipation Models for the Euler Equations," *AIAA Journal*, Vol. 24, No. 12, 1986, pp.1931–1940.

Concentration Measurements in a Transverse Jet by Planar Laser-Induced Fluorescence of Acetone

A. Lozano,* S. H. Smith,* M. G. Mungal,† and R. K. Hanson‡
Stanford University, Stanford, California 94305

I. Introduction

PLANAR laser-induced fluorescence (PLIF) is an attractive technique for concentration measurements in liquid and gaseous flows[1–3] because it is nonintrusive, effectively instantaneous, and provides concentration information in a whole plane without integration along the line of sight. Its use of molecular markers avoids problems of particle lag in fluid flow, and allows high spatial resolution measurements with minimal alteration of the flow conditions. However, although there is a large variety of potential tracers to be used in liquid flows, the selection is somewhat reduced when working with gases, and most chemicals currently used in gaseous PLIF concentration measurements (NO, I_2, biacetyl, or acetaldehyde) are not ideal for common experimental conditions, such as nonreacting turbulent flows at medium-high speeds and standard temperature and pressure. NO and I_2 have obvious toxicity, corrosion, and disposal problems. Acetaldehyde is carcinogenic, whereas biacetyl has a low vapor pressure and a peak absorption at a somewhat undesirable wavelength for current lasers, 420 nm. Recently, Lozano et al.[4] and Lozano[5] demonstrated the use of acetone as a concentration tracer in a small free air jet. Acetone was shown to be a convenient fluorescent marker when working in air flows, providing high signal-to-noise ratios (SNR). In the present work, acetone is used to obtain concentration images in a subsonic transverse air jet. Detection with a highly sensitive charged coupled device (CCD) camera has improved the data quality, decreasing the minimum detectable signal, increasing the SNR, and enabling the successful single-shot imaging of large fields of view (29×29 cm).

II. Tracer

Acetone is a very promising tracer for PLIF concentration measurements in gaseous flows, owing to its physical and photophysical characteristics. It has a high vapor pressure (~180 Torr at 20°C), which allows for high seeding densities, and its absorption band is broad (225–320 nm) with a maximum between 279 and 280 nm ($\sigma = 4.7 \times 10^{-20}$ cm^2). Acetone can, consequently, be excited using different commercially available lasers: a XeCl excimer (308 nm), a frequency-doubled dye laser operating with a red dye (e.g., Rhodamine 560, Rhodamine 590, or Kiton red), a fre-

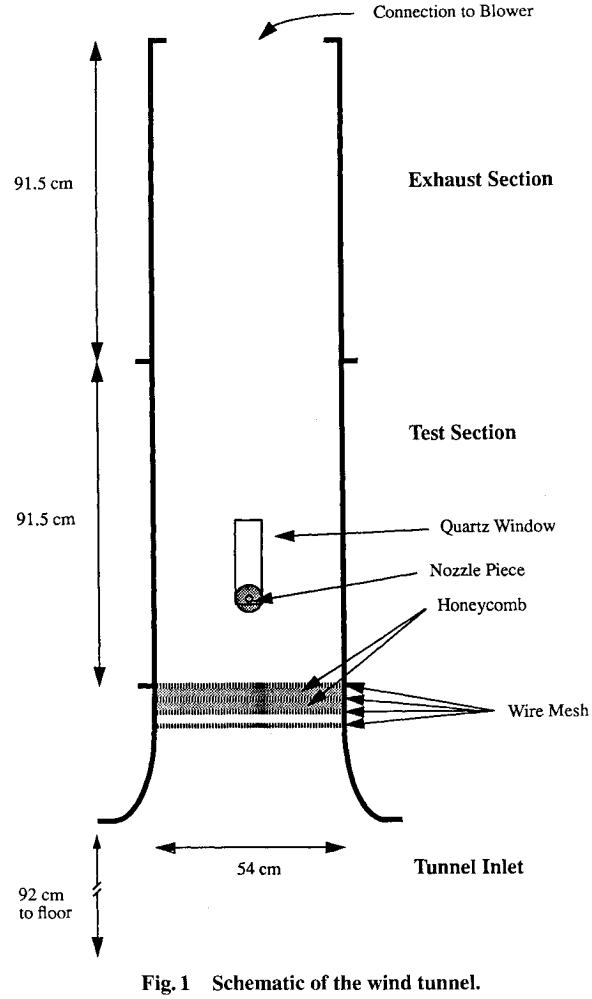

Fig. 1 Schematic of the wind tunnel.

Received Nov. 27, 1992; revision received May 25, 1993; accepted for publication May 26, 1993. Copyright © 1993 by the American Institute of Aeronautics and Astronautics, Inc. All rights reserved.

*Research Assistant, High Temperature Gasdynamics Laboratory, Department of Mechanical Engineering.

†Associate Professor, High Temperature Gasdynamics Laboratory, Department of Mechanical Engineering. Senior Member AIAA.

‡Professor, High Temperature Gasdynamics Laboratory, Department of Mechanical Engineering. Associate Fellow AIAA.

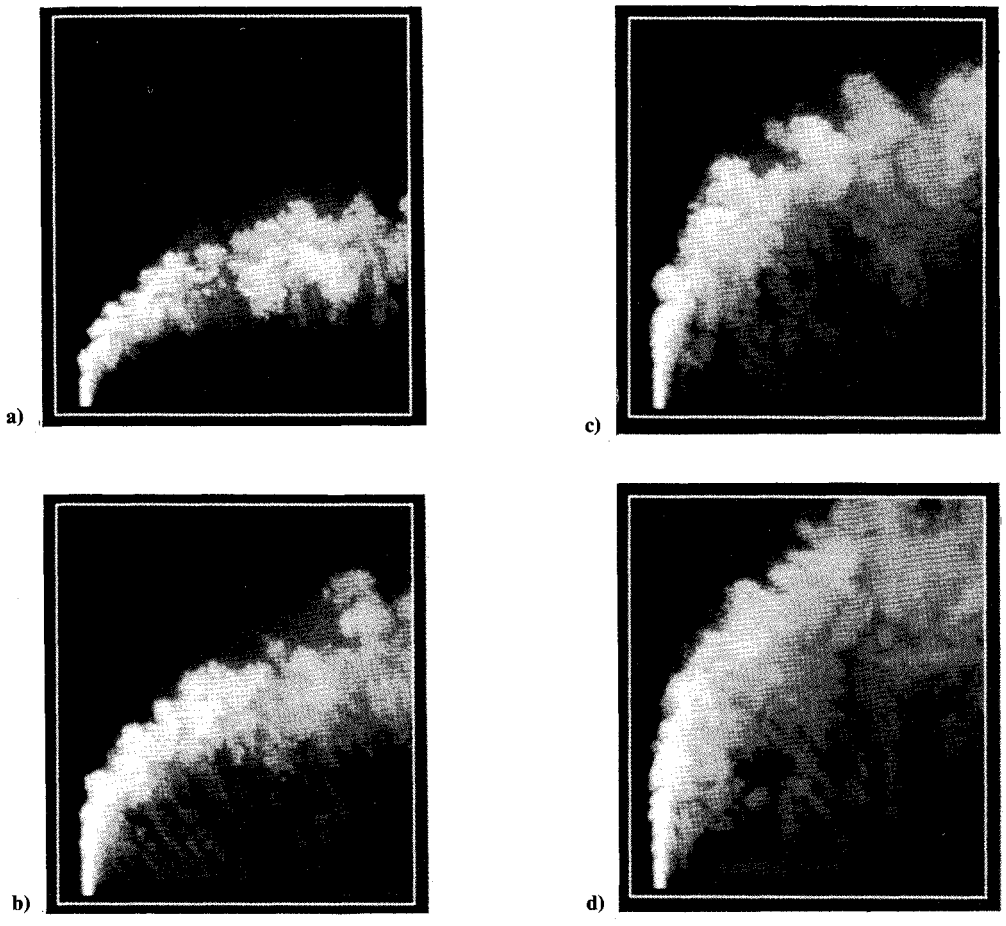

Fig. 2 Instantaneous corrected concentration images of the transverse jet for a crossflow velocity of 7.7 m/s and different jet velocities: a) 55, b) 89, c) 119, and d) 154 m/s; field of view is 25 × 27 cm, nozzle diameter 0.5 cm.

quency quadrupled Nd:YAG (266 nm), or a KrF excimer (248 nm). The use of wavelengths shorter than 250 nm is not ideal because acetone singlet decomposition becomes a competing process with the fluorescence emission. On excitation, acetone fluoresces over a broadband in the blue (350–550 nm), with a peak at 435 nm, an emission efficiency $\phi_f = 0.2\%$, and a short lifetime of ~4 ns, which enables high temporal resolution imaging without the need of gated cameras. Acetone also phosphoresces with a spectrum similar to the fluorescence emission (but extending to longer wavelengths), with a lifetime of 200 μs and an efficiency of 1.8%. Phosphorescence intensity depends on temperature and is strongly quenched by oxygen. The fluorescence, however, is independent of temperature, and insensitive to quenching by air. Acetone toxicity is very mild, and its cost is economical. For a more detailed description of acetone photophysics see Lozano et al.[4] and Lozano.[5]

All of these characteristics made acetone the tracer of choice for the experiments reported here based on imaging of fluorescence emission. Possible interferences by the temperature-dependent phosphorescence are completely negligible when air is used as the carrier gas. Furthermore, as fast shuttering is not required, images can be obtain with higher SNR, dynamic range, and spatial resolution than those attainable with intensified cameras.

III. Experimental Setup

To perform these experiments, a small wind tunnel was designed and built. The wind tunnel, shown in Fig. 1, is a vertical structure 220 cm high with a 54 × 54-cm square cross section. It is suspended from the ceiling of the laboratory and is composed of three parts: the inlet, the test section, and the exhaust. The crossflow travels vertically upward, whereas the jet is injected horizontally. The 91.5-cm-high exhaust section, made of 0.635-cm (1/4-in.) aluminum plate connects to the 5-hp blower that induces the crossflow from the ambient room air. The test section, 91.5 cm tall, is formed by an aluminum frame to which the walls are attached. Two opposite side walls are 0.635-cm(1/4-in.) glass panes, which provide optical access for image acquisition. Note that as acetone fluorescence peaks in the blue, this glass is not required to transmit in the uv. The third wall, made of aluminum, has a 7.6-cm (3-in.) circular hole for the nozzle. The front aluminum wall is a rectangular frame that can be covered by different combinations of rectangular filler plates of various lengths. One of them contains a 24 × 6.3-cm quartz piece to transmit the excitation laser sheet. This plate can be rotated to allow the laser sheet to cut the flow axially or transversely, and displaced vertically to image different downstream regions of the flow.

The tunnel inlet has a contraction of elliptical profile. Four wire-mesh screens and two honeycomb plates are used to homogenize and condition the crossflow. The crossflow velocity is constant, set by the blower to be 7.7 m/s, with a 1% turbulence intensity and less than a 5% velocity variation. The jet/crossflow velocity ratio can be modified by varying the jet velocity. The jet inlet, attached to the side wall of the tunnel, consists of a cylindrical 16.5 × 25.4-cm settling chamber containing two perforated plates and two honeycomb screens equally spaced, with a 0.5-cm-diam contoured nozzle at the end of the chamber that communicates with the tunnel test section.

A model number SLL 8000 Candela flashlamp-pumped dye laser, circulating Rhodamine 590 Chloride, was used to excite the acetone. The output emission was tuned to 590 nm and frequency-doubled with an ammonium dihydrogen phosphate crystal. Nominally, this laser is capable of a maximum energy per pulse over 10 J in the fundamental frequency (operating without etalons), resulting in ~1 J/pulse for the frequency-doubled emission. However, for safety reasons, the laser was operated with a 50/50 mixture of methanol and water, instead of using pure methanol as the solvent. This substantially reduces the energy output in the fundamental frequency and the doubling crystal conversion efficiency; as a re-

sult, we were only able to obtain 150 mJ/pulse at 295 nm. The pulse duration is 2 μs, which can be desirable to reduce the risks of absorption saturation. For very fast flows these long pulses can cause motion blurring, although this was not the case in the measurements that will be presented, where the fastest speed was 154 m/s.

The image collection system was comprised of a Photometrics AT 200 controller (16 bit analog-to-digital converter), a thermoelectrically cooled (−40°C) CH250 camera head with a Tektronix TEK 512CB/MPP CCD array, and a Nikon 50 mm F 1.2 lens. This array is a 512×512 pixels, thinned, backside-illuminated CCD detector, with a pixel size of 27 μm, and was operated in multiphase pinned mode to reduce the dark current. Thinned, backside-illuminated detectors have a much higher quantum efficiency than similar thick, frontside-illuminated arrays. This difference is especially significant for blue light, where efficiencies increase from 10–15% in frontside-illuminated devices to values as high as ~50% at 450 nm and ~55% at 400 nm. The Photometrics 200 system has a reported total noise of 13 e^- with a reported gain factor of 4 e^-/analog to digital units.

IV. Experimental Conditions

The images were acquired by cutting the flow axially through the nozzle centerline. The laser sheet was formed into a slightly divergent sheet, 25–27 cm high and 3 mm thick. The imaged field of view was 29×29 cm. A short-wavelength-pass interference filter (cutoff at 567 nm) was placed in front of the camera to decrease the background signal produced by emission at the fundamental frequency (590 nm).

The crossflow velocity was maintained at a constant value of 7.7 m/s. Images were acquired for five different jet velocities: 55, 89, 98, 119, and 154 m/s, corresponding to the following Reynolds numbers: 18,000, 30,000, 33,000, 40,000, and 51,000, and jet-to-crossflow speed ratios $r = V_j/V_{cf}$ of 7.1, 11.5, 12.7, 15.4, and 20.

Acetone was seeded by bubbling the carrier air into a bottle containing the liquid. To filter acetone droplets, a 40 μm micropore filter was attached at the container exit. To avoid fluctuations in the acetone seeding density due to the temperature decrease caused by evaporation, the bottle was immersed in a thermostatic bath.

V. Results

Four corrected instantaneous images are presented in Fig. 2 corresponding to four different jet exit velocities: 55, 89, 119, and 154 m/s. They are displayed with a 2.5 gamma exponential color table of the form $I_{corr} = I^{1/\gamma}$, where I is the intensity linearly dependent on the acetone concentration and I_{corr} the intensity mapped through the color table, to better distinguish the details in the wake region. These images have peak signal-to-noise ratios

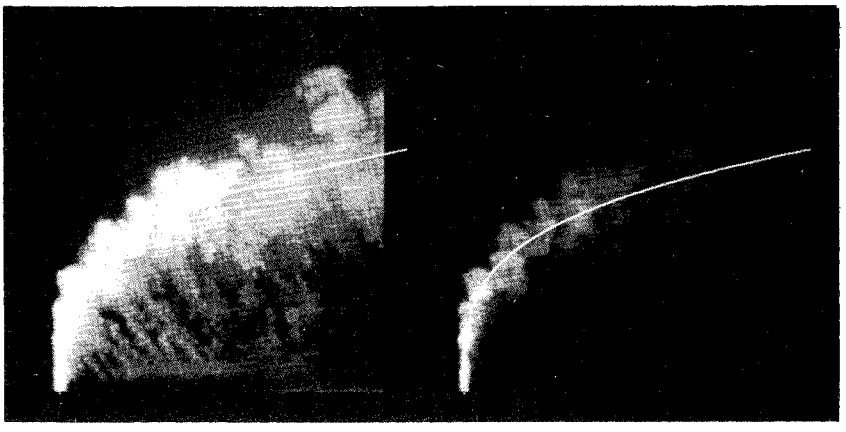

Fig. 3 Instantaneous concentration image for a jet-to-crossflow velocity ratio r = 11.5 with a calculated average centerline location superposed; the image is displayed with an exponential color table (left) and a linear grey scale (right).

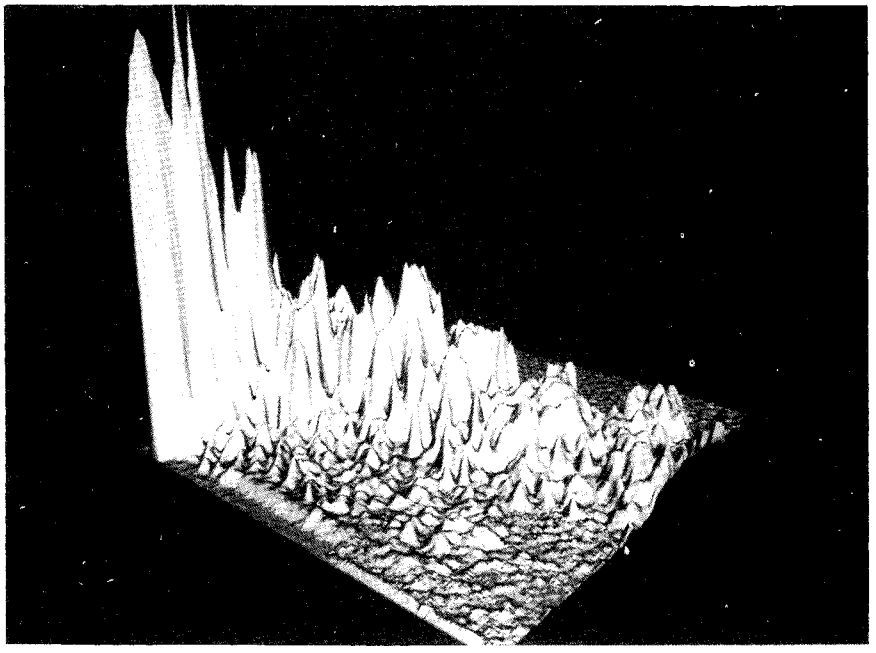

Fig. 4 Landscape rendering of the same image displayed in Fig. 3 (right), after application of a 3×3 smoothing filter.

over 200 with signal dynamic ranges of ~225, which are much lower than the potentially maximum ranges, and which were partly limited by the high background levels caused by the laser. As can be expected, the penetration distance increases with the jet-to-freestream velocity ratio. The spreading of the jet is also seen to increase as the velocity ratio increases toward 20:1, where the jet flame length as defined by Broadwell and Breidenthal[6] should be a minimum.[7] The most interesting features in all of these images are, however, the "fingers" that separate from the jet and travel toward the wall in the wake region. The jet fluid concentration of these structures is quite low, and in some cases they might be buried in the background noise of a poor detection system. If the images are displayed with a linear gray scale, nothing between the jet and the tunnel wall can be discerned (see Fig. 3).

The instantaneous images have been compared to an average jet centerline trajectory calculated with the expression (see Pratte and Baines[8])

$$\frac{y}{rd_0} = 2.05^* \left(\frac{x}{rd_0}\right)^{0.28}$$

where r is the jet-to-crossflow ratio and d_0 is the source diameter, for r ranging from 5 to 35. Figure 3 displays an instantaneous image (with $r = 11.5$) on which the calculated jet centerline location, obtained with the preceding formula, is superposed. The same excellent agreement between calculated and measured jet positions has been observed for the other r values studied.

Although eddies of crossflow fluid penetrating the jet have been previously observed,[9,10] the opposite case, which is found in out-images (jet fluid entering the wake), has to our knowledge never been reported. Furthermore, the absence of this jet/crossflow interaction was interpreted by Fric and Roshko[9] as evidence that the jet vorticity does not contribute to the wake vorticity. It is possible, however, that they were not able to detect these structures due to a lack of sensitivity in their experiments (smoke-wire visualization). It is also possible that some jet fluid may flow axially into the cores of the wake vortices once they have formed.[11] In any event, more images are required to formulate any statement about these wake detachments; e.g., what are the conditions determining their presence, their possible dependence on velocity ratio or jet Reynolds number, orientation with respect to the jet and wall, etc.

In Fig. 4, the same image shown in Fig. 3 (right) is displayed as a rendered surface where intensities have been mapped into heights. Prior to the rendering, a 3×3 smoothing filter was applied to the original image to decrease noise fluctuations. This type of presentation facilitates the visual analysis of gradient magnitudes and quantitative distribution of fluid concentration. This jet centerline concentration decay is easily observed, together with the existence of areas of nearly uniform concentration. The complexity of smaller scale details is also evidenced, whereas the wake region is more readily discernible.

The results presented here provide confirmation of the utility of PLIF imaging of acetone for fundamental studies in fluid mechanics, and also suggest the need for a more detailed investigation that could lead to deeper understanding of scalar mixing in transverse jets. Because the interesting features involve low concentrations, it is essential to use high-sensitivity detectors. A thin, backside-illuminated CCD array can be considered the "state of the art" device for this type of measurement, especially when imaging acetone fluorescence. To maximize the emitted signal, however, high energy excitation lasers should still be used.

Acknowledgments

This work has been sponsored by the Air Force Office of Scientific Research, Aerospace Sciences Directorate, with Julian Tishkoff as the technical monitor. S. H. Smith is supported by the NDSEG fellowship.

References

[1]Dimotakis, P. E., Miake-Lye, R. C., and Papantoniou, D. A., "Structure and Dynamics of Round Turbulent Jets," *Physics of Fluids,* Vol. 26, No. 11, 1983, pp. 3185–3192.

[2]Hanson, R. K., Seitzman, J. M., and Paul, P. H., "Planar Laser-Induced Fluorescence Imaging of Combustion Gases," *Applied Physics B,* Vol. 50, No. 6, 1990, pp. 441–454.

[3]van Cruyningen, I., Lozano, A., and Hanson, R. K., "Quantitative Imaging of Concentration by Planar Laser Induced Fluorescence," *Experiments in Fluids,* Vol. 10, No. 1, 1990, pp. 41–49.

[4]Lozano, A., Yip, B., and Hanson, R. K., "Acetone: a Tracer for Concentration Measurements in Gaseous Flows by Planar Laser-Induced Fluorescence," *Experiments in Fluids,* Vol. 13, 1992, pp. 369–376.

[5]Lozano, A., "Laser- Excited Luminescent Tracers for Planar Concentration Measurements in Gaseous Jets," High Temperature Gas Dynamics Lab. Rept. T-284, Stanford Univ., Stanford, CA, 1992.

[6]Broadwell, J. E., and Breidenthal, R. E., "Structure and Mixing of a Transverse Jet in Incompressible Flow," *Journal of Fluid Mechanics,* Vol. 148, Nov. 1984, pp. 405–412.

[7]Karagozian, A. R., "The Flame Structure and Vorticity Generated by a Chemically Reacting Transverse Jet," *AIAA Journal,* Vol. 24, No. 9, 1986, pp. 1502–1507.

[8]Pratte, B. D., and Baines, W. D., "Profiles of the Round Turbulent Jet in a Cross Flow," *Journal of the Hydronautical Division of the American Society of Civil Engineers,* Vol. 92, Nov. 1967, pp. 53–64.

[9]Fric, T. F., and Roshko, A., "Structure in the Near Field of the Transverse Jet," 7th Symposium on Turbulent Shear Flows, Paper 6-4, Stanford, CA, Aug. 1989.

[10]Fric, T. F., "Structure in the Near Field of the Transverse Jet," Ph.D. Thesis, California Inst. of Technology, Pasadena, CA, 1990.

[11]Roshko, A., private communication, California Inst. of Technology, Pasadena, CA, 1993.

Effects of In-Plane Displacements on Frequency and Damping of Composite Laminates

Kyo-Nam Koo* and In Lee†
Korea Advanced Institute of Science and Technology, Taejon 305-701, Republic of Korea

Introduction

TRANSVERSE shear deformation plays an important role in anisotropic plates since most of the advanced composites have a low ratio of the transverse shear modulus to the modulus in the fiber direction. Although the shear deformation plate theory is adequate for predicting the global responses of medium-thick laminated plates such as deflection, natural frequency, and buckling load, it fails to give accurate predictions for transverse shear stresses and in-plane displacements. The fact that the damping characteristics are affected by the local behavior of plate deformation whereas the natural frequency is determined by global deformation requires a refined theory for the damping analysis of composite laminated plates.

The various approaches used for modeling multilayered composite plates were reviewed by Noor and Burton.[1] The fundamental frequency and the associated mode shape of free-vibration problems were considered in several papers.[2,3] However, the effect of the in-plane displacements on the damping characteristics of composite laminates has not been studied in the previous papers. Research on the damping analysis of composite plates is not so extensive as that on the undamped free-vibration analysis. Lin et al.[4] used a damped element model to evaluate the specific damping capacity (SDC) of composite plates. In spite of the great contribution their work made to this field of study, the effect of the

Received Jan. 14, 1993; revision received May 28, 1993; accepted for publication May 30, 1993. Copyright © 1993 by the American Institute of Aeronautics and Astronautics, Inc. All rights reserved.

*Graduate Research Assistant, Department of Aerospace Engineering, 373-1, Kusong-dong, Yusong-gu.

†Associate Professor, Department of Aerospace Engineering, 373-1, Kusong-dong, Yusong-gu. Member AIAA.